applied sciences

MDPI

Article

Analysis of the Effect of the Tool Shape on the Performance of Pre-Cutting Machines during Tunneling Using Linear Cutting Tests

Han-eol Kim [1], Kyoung-min Nam [1], Tae-su Kyeon [2], Hafeezur Rehman [3] and Han-kyu Yoo [1,*]

[1] Department of Civil and Environmental Engineering, Hanyang University, 55 Hanyangdaehak-ro, Sangnok-gu, Ansan 15588, Korea; k2k402r@hanyang.ac.kr (H.-e.K.); namkm@hanyang.ac.kr (K.-m.N.)
[2] Department of Infra Division Sinansan Line Section 2, Posco E&C, 38 Namwang-gil, Siheung 14985, Korea; tskyeon@poscoenc.com
[3] Department of Mining Engineering, Baluchistan University of Information Technology Engineering and Management Sciences (BUITEMS), Quetta 87300, Pakistan; miner1239@yahoo.com
* Correspondence: hankyu@hanyang.ac.kr; Tel.: +82-31-400-5147; Fax: +82-31-409-4104

Abstract: Owing to several advantages, mechanical pre-cutting techniques were first introduced in the United States and subsequently used in Europe for tunneling. Pre-cutting machines perform mechanical excavation tunneling using cutting tools such as tunnel boring machines (TBMs) and roadheaders. Linear cutting tests are reliable and widely used to predict the performance of TBMs and roadheaders. In this study, the effect of the cutting tool shape of a pre-cutting machine was analyzed using linear cutting tests. Assuming the basic shape of the tool, the clearance and rake angles of the tool were designated as variables that determine the shape. The experimental results for samples with different mechanical properties were analyzed considering the cutting force, cutting volume, and specific energy, which were inversely related to the clearance angle. Initially, the force decreased significantly as the clearance angle increased from 0° to 5°, and then converged at angles of 10° and higher. However, the cutting volume decreased linearly with angles. The specific energy behaved similarly to the force. Compared with the clearance angle, the rake angle slightly affected the cutting force, volume, and specific energy. When the rake angle increased from 0° to 5°, the cutting force and volume decreased slightly; however, both increased after 5°. The specific energy exhibited a similar trend.

Keywords: pre-cutting machine; cutting tool; cutting force; cutting volume; specific energy; linear cutting test

Citation: Kim, H.-e.; Nam, K.-m.; Kyeon, T.-s.; Rehman, H.; Yoo, H.-k. Analysis of the Effect of the Tool Shape on the Performance of Pre-Cutting Machines during Tunneling Using Linear Cutting Tests. *Appl. Sci.* **2022**, *12*, 4489. https://doi.org/10.3390/app12094489

Academic Editor: Tiago Miranda

Received: 4 April 2022
Accepted: 26 April 2022
Published: 28 April 2022

1. Introduction

The mechanical pre-cutting method was first introduced as a tunneling technique in the United States in 1950 and applied in traffic tunnels in France in the 1970s [1]. Since then, it has been widely used in Europe. In the 1980s and 1990s, this technique was used in approximately 30 tunnels in France and Italy [2]. The mechanical pre-cutting method is economical and effective for rocks with a strength of up to 70 MPa and can be applied up to a compressive strength of 100 MPa for a short distance [1]. This technique improves the quality and stability of tunneling, reduces ground settlement, noise and vibration, and accelerates excavation [3]. This tunneling method involves a pre-cutting machine, as shown in Figure 1, that uses a cutting arm that resembles a chainsaw as a cutter. As the cutting arm moves along the pinion track, a precut is formed in the shape of the tunnel to be excavated. Recently, this machine has been developed as an excavation equipment called a tunnel widening machine (TWM), which is also used to enlarge existing tunnels [4,5].

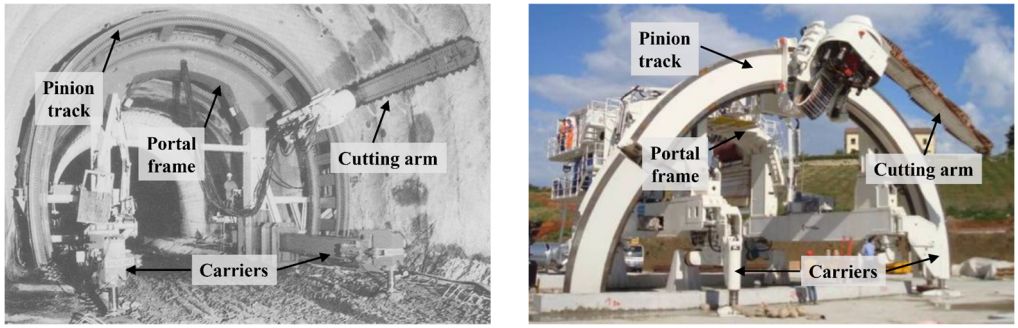

(**a**) (**b**)

Figure 1. Pre-cutting machine: (**a**) in a double track railway tunnel (Reproduced with permission from Ref. [1]. 1991. E. van Walsum); (**b**) for enlargement (Reproduced with permission from Ref. [4]. 2014. Lunardi et al.).

Similar to tunnel boring machines (TBMs) and roadheaders, pre-cutting machines can also be classified as tunnel excavation machines that use cutting tools. Cutting tools can be broadly classified into roller and drag types. The disc cutter is a roller type, while the drag type typically comprises a conical and chisel pick [6]. A linear cutting test is widely used to design the cutter head of such excavation equipment for evaluating the performance of such tools [7]. Therefore, various studies have been conducted on cutting tools using linear cutting tests to improve the excavation efficiency of excavation machines.

Various studies have been conducted to evaluate and analyze the effects of the parameters related to the shape of the cutting tool using a linear cutting test. Roxborough and Phillips [8] performed linear cutting tests on V-type disk cutters with varying diameters, edge angles, and penetration depths, and proposed a cutter force prediction model. Subsequently, various studies have confirmed that a constant cross-section (CCS)-type disc cutter is more effective with high rock-cutting efficiency and low tool wear [9–11]. Nishimatsu [12] proposed a model for predicting cutting force by analyzing the theoretical and experimental values for chisel picks with rake angles of 10°, 20°, 30°, and 40°. Wang et al. [13] analyzed the effects of the clearance angle, rake angle, and penetration depth on the cutting force and specific energy using five types of conical picks and proposed an empirical model accordingly. Aresh et al. [14] analyzed the rock chip formation mechanism by varying the rake angle of the drag type cutting tool. The literature reveals that although several studies have been conducted on the shape of disc cutters and pick cutters, there have been no comprehensive studies on the cutting tools of pre-cutting machines. In order to increase the excavation efficiency of the pre-cutting machine, research on the shape of the cutting tool is essential.

The contribution to this study is that it can be a reference in determining the cutting tool shape of a pre-cutting machine that could improve cutting efficiency. The linear cutting test was performed to analyze the effect of the shape of the cutting tool of the pre-cutting machine. Because pre-cutting machines do not have uniformly shaped cutting tools, such as TBMs or roadheaders, the basic shape of the cutting tool is assumed. The clearance and rake angles were considered as variables in this study, and tests were performed by changing the compressive strength of the rock specimen and depth of the cut. The shape effect was analyzed by focusing on the cutting force generated by cutting rocks of different strengths. Moreover, cutting volume and specific energy were also analyzed.

2. Materials and Methods

2.1. Linear Cutting Machine

The linear cutting test is performed with a linear cutting machine. Figure 2 shows the overall appearance of the servomotor-driven linear cutting test machine used in this study. The two main parts of the machine are a cutting system and a computer for controlling the equipment and checking and storing the experimental data. Unlike the widely used

hydraulic linear cutting machines [15–20], this machine can control the moving distance of the rock and cutting tool more precisely. The bucket that holds the rock sample can be moved along the *x*-and *y*-axes using a servomotor that can move up to 100 mm/s. The *z*-axis servomotor moves the cutting tool to control the penetration depth.

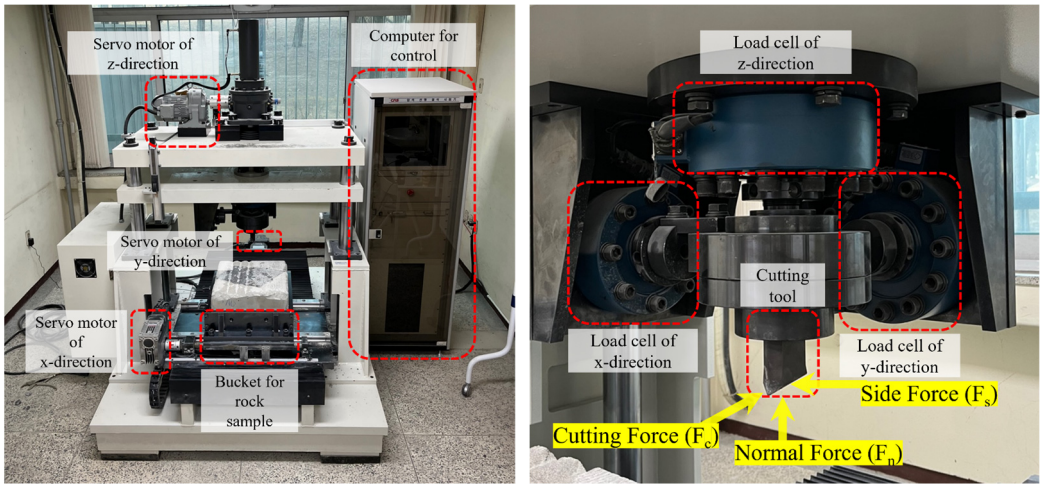

(**a**) (**b**)

Figure 2. Linear cutting machine (LCM): (**a**) overview of LCM; (**b**) load cells and cutting tool.

Generally, a three-axis load cell capable of measuring all three directional forces with one cell is used [15–20]. However, in this study, three load cells were installed along the *x*, *y*, and *z* axes. The *y*-axis and *z*-axis load cells, which measure the cutting force (F_c) and normal force (F_n), respectively, can measure loads of up to 25 t. A load cell with a capacity of 15 t was used as the *x*-axis to measure the side force (F_s) (Figure 2b).

Software for checking the measured values and test progress in real time was installed on the control computer to set the servomotor speed and measurement interval of the load cell.

2.2. Cutting Tool of the Pre-Cutting Machine

The cutting arm of the pre-cutting machine, which resembled a chainsaw, performed the excavation as shown in Figure 1. Here, the cutting tool performs the same role as the saw blade of the chainsaw in the cutting arm.

In this study, the basic shape of the cutting tool was assumed, as shown in Figure 3. The height (h), thickness (t), width (d), and edge angle (θ) were assumed to be 80 mm, 40 mm, 60 mm, and 120°, respectively. The edge of the cutting tool in contact with the rock was filleted with a radius of 2 mm. The cutting tool was made of SKD11 alloy steel, and the hardness was HRC60. The surface of the tool was coated with hard chrome plating.

Among the various parameters that determined the shape, the clearance and rake angles were set as variables. Altogether, four cases were considered for clearance angles (α) at intervals of 5° from 0° to 15°, while five cases were considered for rake angle (β) at intervals of 5° from 0° to 20°. As shown in Table 1, the cutting tool was named C00R00 according to the clearance and rake angles. Here, the two numbers after C and R represent the clearance and rake angles, respectively.

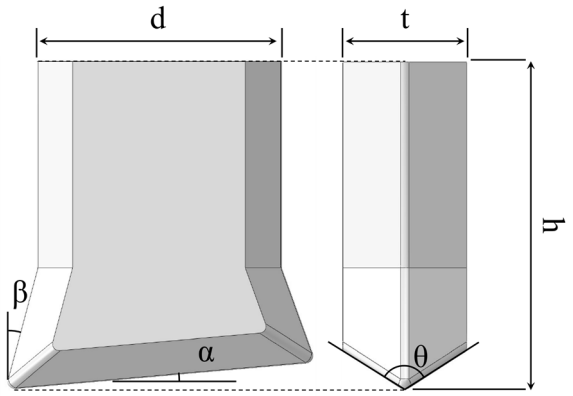

Figure 3. Basic shape of a cutting tool.

Table 1. Names and specifications of the cutting tools.

Name	Clearance Angle, α (Deg.)	Rake Angle, β (Deg.)
C00R20	0	20
C05R20	5	20
C10R20	10	20
C15R20	15	20
C05R00	5	0
C05R05	5	5
C05R10	5	10
C05R15	5	15

2.3. Rock Sample

Mechanical pre-cutting is effective at compressive strengths of 70 MPa or less [1]. Therefore, cutting tests were conducted on the rocks under a pressure of 50 MPa. However, owing to the great difficulty in obtaining actual rocks of the desired strength, rock models of various strengths were manufactured using mortar, cement, and sand. The model rocks measured 400 mm × 400 mm × 300 mm. Four rocks were manufactured, targeting uniaxial compressive strengths (UCS) of 20 MPa, 30 MPa, 40 MPa, and 50 MPa.

The uniaxial compression tests and brazilian tests were used to verify that the manufactured rock had reached the target strength. Table 2 lists the physical and mechanical properties of model rocks with different strengths.

Table 2. Physical and mechanical properties of the model rocks.

Target Strength (MPa)	Elastic Modulus (GPa)	Density (kg/m^3)	Poisson's Ratio	Uniaxial Compressive Strength, UCS (MPa)	Brazilian Tensile Strength, BTS (MPa)
20	16.92	2214	0.3	18	2.06
30	33.35	2363	0.3	29.3	2.18
40	38.92	2382	0.3	42	2.51
50	44.47	2235	0.3	51.8	2.99

2.4. Linear Cutting Test

When the rock was cut using a cutting tool, the three-axis reaction forces, namely, the cutting, normal, and side forces, were measured, as shown in Figure 2b. In general, cutting forces are related to the torque and specific energy of the tunnel excavation machine. The normal force is related to the thrust force and capacity of the machine, whereas the side forces are related to its vibration and stability [17].

Tunnel excavation machines, such as tunnel boring machines (TBMs) and roadheaders, use the concept of specific energy when determining excavation efficiency. The specific energy is the energy required to cut a unit volume, and its lower values indicate high excavation efficiency. This energy can be obtained using Equation (1):

$$SE = \frac{F_c \times l}{V} \quad (1)$$

where
SE = specific energy (J/m^3);
F_c = average cutting force (N);
l = cutting length (m);
V = cutting volume (m^3).

The equation reveals that the specific energy is significantly affected by the cutting force and cutting volume. Considering these influencing factors, this study focuses on the cutting force, cutting volume, and specific energy. Since the cutting speed of the rock had no apparent effect on the cutting performance [17,21], it was maintained at 12.5 mm/s, and the force was measured every 25 ms.

The cutting volume was measured and analyzed only for rocks at 40 and 50 MPa. The volume was measured by scanning the surface of the rock after cutting using a Calibry mini from Thor3d (Figure 4).

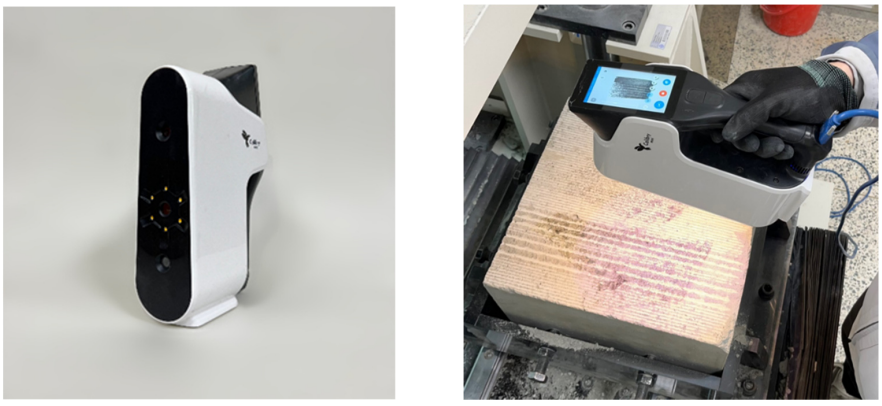

(**a**) (**b**)

Figure 4. 3D scanning for volume measurement: (**a**) Calibry Mini and (**b**) example of 3D scanning.

Cutting tests were performed on each rock model using the cutting tools listed in Table 1. The cutting depth was set to 3, 6, and 9 mm, and at least three cuts were made. The s/p ratio, which is the ratio of cutting spacing and depth, was set to nine or more to avoid interaction between cuttings (Figure 5).

(**a**) (**b**) (**c**)

Figure 5. Cutting spacing by penetration depth: (**a**) depth: 3 mm, spacing: 30 mm, (**b**) depth: 6 mm, spacing: 55 mm, and (**c**) depth: 9 mm, spacing: 85 mm.

3. Results

3.1. Relation of the Cutting Force and Rock Chips Generation

The three-axis reaction force occurs when the cutting tool cuts the rock while moving parallel to the rock surface, the cutting force parallel to the cutting direction, normal force perpendicular to the cutting surface, side force perpendicular to the cutting direction and parallel to the cutting surface. Figure 6a shows the cutting, normal, and side forces generated during the experiment. The cutting force, which is related to the generation of rock fragments of various sizes (Figure 6b,c), decreases rapidly when a large rock chip is generated. This can be considered to indicate the generation of rock chips and small particles [6].

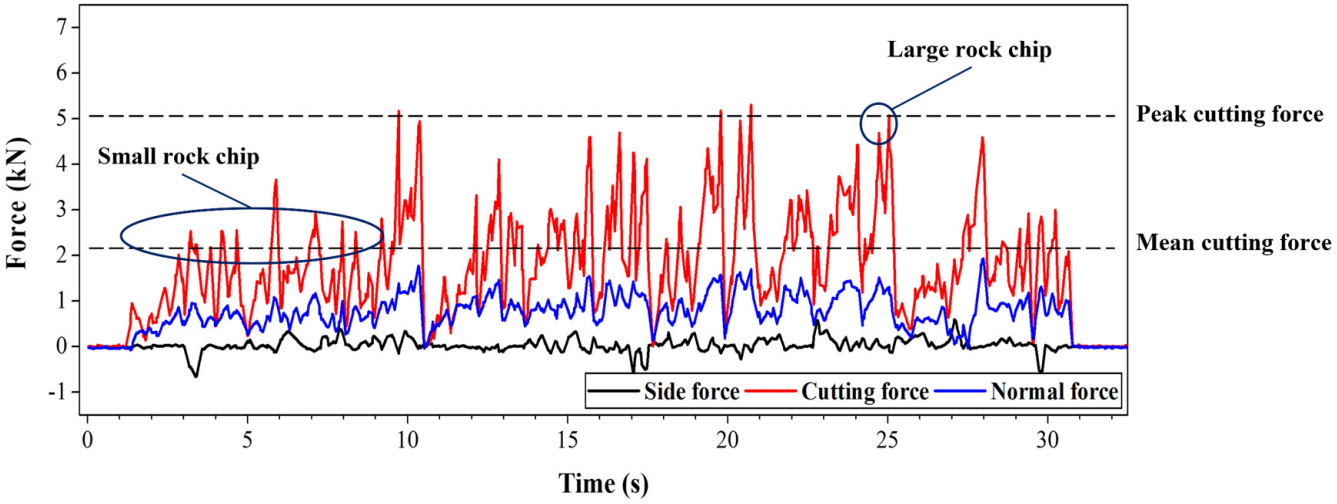

(**a**)

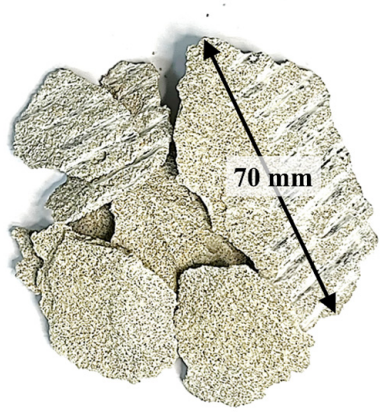

(**b**)

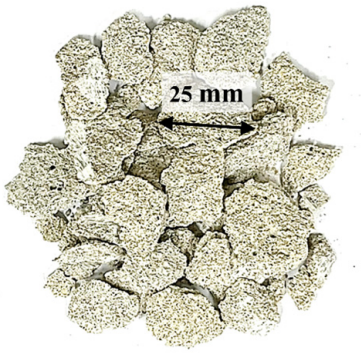

(**c**)

Figure 6. Cutting forces and rock chips generated during the experiment: (**a**) cutting forces during the generation of rock chips, (**b**) large rock chips, and (**c**) small rock chips.

Figure 7 shows the effect of the clearance angle and cutting force generated by cutting the rock with a UCS of 30 MPa. Overall, the maximum cutting force is generated when the clearance angle is 0°, and decreases as the angle increases, with the minimum value occurring at 15°.

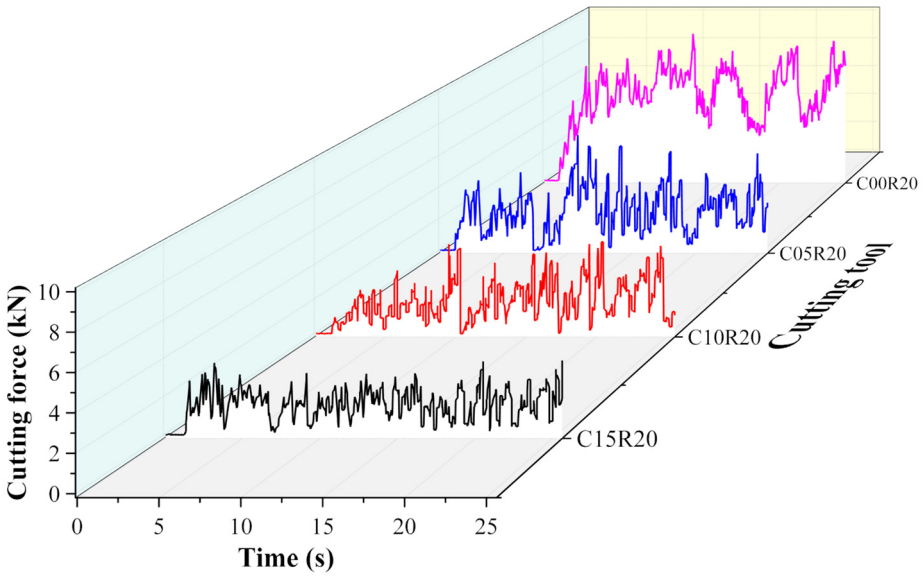

Figure 7. Variation in the cutting force with time for each clearance angle.

When cutting was performed using C00R20, as shown in Figure 7, the sharp drop point of the cutting force was relatively small compared with the other cases. During cutting by C05R20, the sharp drop point of the cutting force increased compared with that of C00R20, but no significant change occurred with the increase in the clearance angle. Therefore, when the clearance angle is 0°, generating small fragments is the main factor in rock cutting, rather than generating large rock chips.

This seems to be a phenomenon caused by the friction between the cutting tool and rock. If the clearance angle is 0°, the contact surface between the cutting tool and rock increases significantly, and the friction force increases significantly. This friction makes the cutting surface wider and smoother and produces small and fine rock chips [13].

The effect of friction can also be confirmed by the sharp decrease in the cutting force while generating rock chips. In the case of the cutting tool with a clearance of 5° or more, the cutting force decreased by 85% on average after the rock chips were generated. However, when the clearance was 0°, the reduction was only 55%, owing to friction.

The variation in the cutting force with respect to the rake angle is shown in Figure 8. Overall, the cutting force increases with the rake angle. However, the effect was small compared with that of the clearance angle. The rock chip produced by cutting did not change significantly despite the change in angle.

3.2. Effect of the Clearance Angle on the Cutting Force

To investigate the effect of the clearance angle, an analysis was performed on the cutting force. The mean cutting force, which is the average value of cutting force generated during cutting, and the peak cutting force, which is the maximum value of cutting force generated during cutting, were analyzed.

Figure 9 shows the mean cutting force generated by each cutting depth and clearance angle. As shown in Figure 9, the cutting force decreases as the clearance angle increases. In particular, when the clearance angle increases from 0° to 5°, the cutting force decreases significantly. When a rock of UCS 20 MPa was cut with a cutting depth of 3 mm, the mean cutting force decreased by 81% from 4.74 kN to 0.88 kN, while in the case of the UCS 50 MPa rock, it decreased by 65% from 8.66 kN to 3.02 kN (Figure 9a). At a cutting depth of 9 mm, it decreased by 67% from 14.45 kN to 4.84 kN and by 56% from 27.28 kN to 12.02 kN for UCS 20 MPa and UCS 50 MPa, respectively (Figure 9c). Thus, the sharp decrease in the mean cutting force owing to the clearance angle appears less as the depth of cut and UCS increase.

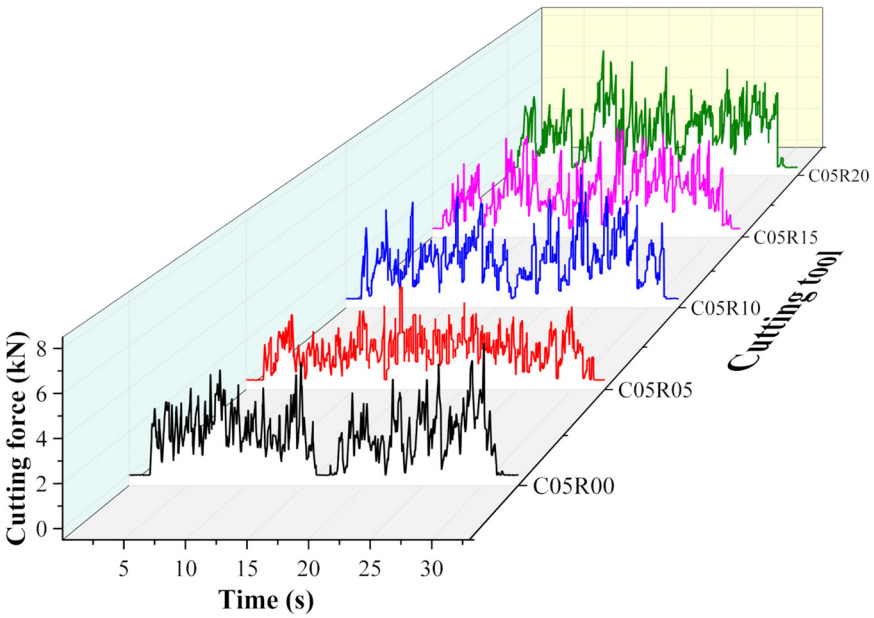

Figure 8. Variation in the cutting force with time for each rake angle.

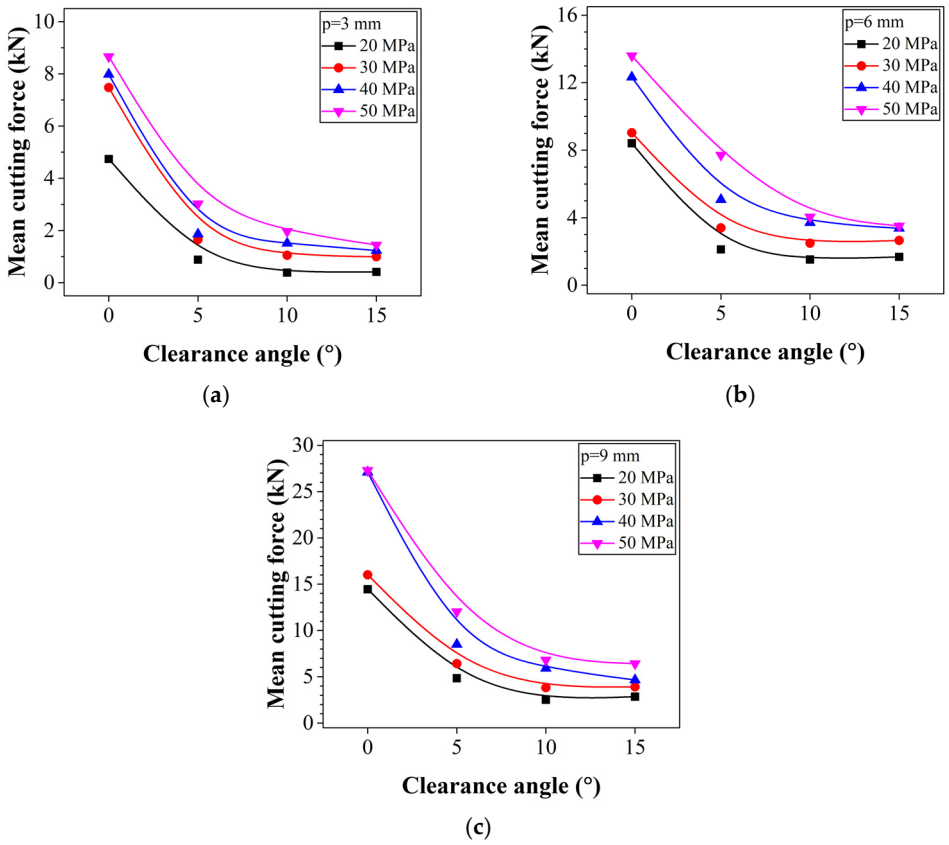

Figure 9. Relationship between the mean cutting force and clearance angle cutting depths (*p*) of: (**a**) 3 mm, (**b**) 6 mm, and (**c**) 9 mm.

When the clearance angle was increased from 5° to 10°, the mean cutting force decreased significantly. Subsequently, if it increases to 10° or more, the cutting force converges to a constant value. When the cutting depth is 6 mm, the average cutting force converges to about 2.5 kN and 3.5 kN for the rocks with UCS of 30 MPa and 40 MPa, respectively (Figure 9b).

The peak cutting force also exhibited changes similar to those of the mean cutting force (Figure 10). For cutting depths of 3 mm, when the clearance angle is increased from 0° to 5°, the peak cutting force reduces by 71% from 8.47 kN to 2.44 kN for the rock with a UCS of 20 MPa. For the same increase in the clearance angle increase and same cutting depth, the peak cutting force decreases by 47% from 11.28 kN to 5.94 kN for the rock with a UCS of 50 MPa (Figure 10a). When the cutting depth is 9 mm, it reduces by 69% from 30.8 kN to 9.65 kN and and 45% from 43.99 kN to 24.05 kN for rocks with USC of 20 MPa and 50 MPa, respectively (Figure 10c). However, the reduction was smaller than that of the average cutting force.

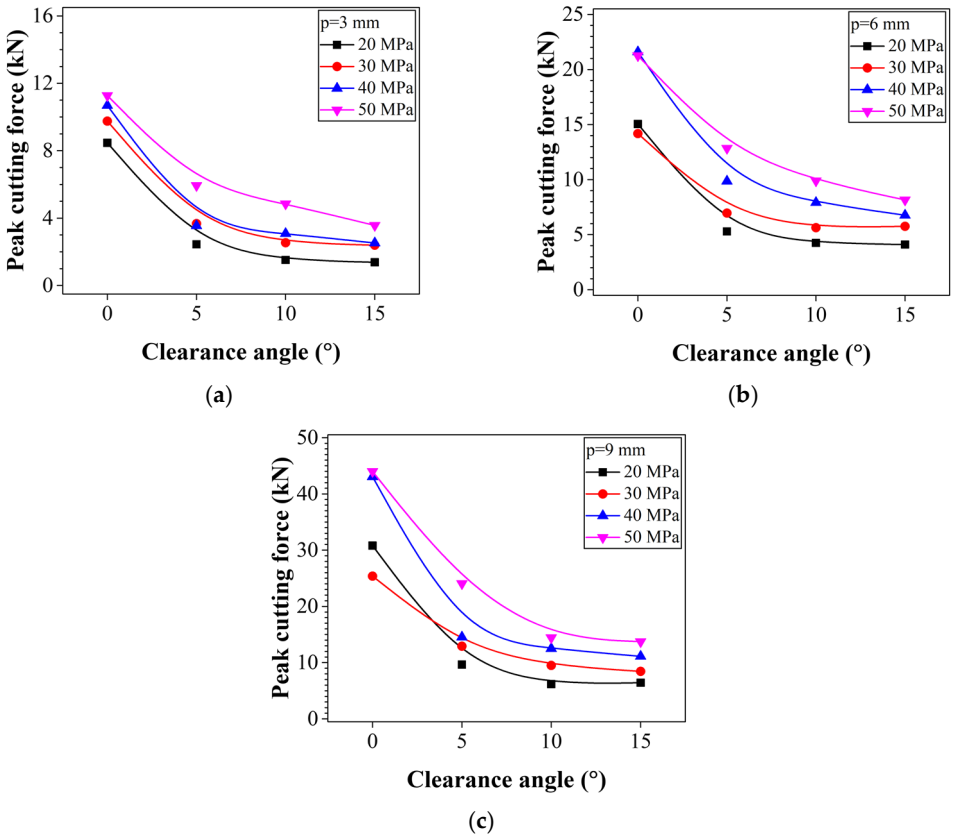

Figure 10. Relationship between the peak cutting force and clearance angle for cutting depths (*p*) of: (**a**) 3 mm, (**b**) 6 mm, and (**c**) 9 mm.

Even when the clearance angle increased above 10°, the cutting force converged to a constant value equal to the mean cutting force. When the cutting depth was 6 mm, it converged to about 5.6 kN and 6.8 kN for the rock samples of UCS 30 MPa and UCS 40 MPa, respectively (Figure 10b). The details of the mean and peak cutting forces according to the clearance angle are listed in Table 3.

This phenomenon also seems to be caused by the friction between the cutting tool and rock. If the clearance angle is increased from 0° to 5°, the contact surface with the rock is significantly reduced, resulting in a sharp decrease in cutting force. If the angle exceeds 5°, it appears to converge to a constant value because the decrease in the contact surface is insufficient to significantly affect the frictional force.

Table 3. Mean and peak cutting forces for various clearance angles.

UCS (MPa)	p (mm)	Clearance Angle (Deg.)							
		0		5		10		15	
		F_c (kN)	F'_c (kN)	F_c (kN)	F'_c (kN)	F_c (kN)	F'_c (kN)	F_c (kN)	F'_c (kN)
20	3	4.74	8.47	0.88	2.44	0.39	1.52	0.41	1.38
	6	8.42	15.05	2.12	5.30	1.53	4.25	1.68	4.11
	9	14.45	30.80	4.84	9.65	2.52	6.18	2.85	6.43
30	3	7.48	9.75	1.65	3.68	1.05	2.54	0.99	2.40
	6	9.04	14.18	3.40	6.96	2.49	5.64	2.65	5.76
	9	16.00	25.37	6.42	12.92	3.82	9.50	3.91	8.45
40	3	7.98	10.68	1.86	3.55	1.51	3.08	1.23	2.53
	6	12.33	21.60	5.07	9.86	3.71	7.92	3.37	6.77
	9	27.09	43.05	8.50	14.54	5.91	12.50	4.66	11.12
50	3	8.66	11.28	3.02	5.94	1.97	4.85	1.45	3.57
	6	13.59	21.25	7.71	12.85	4.05	9.89	3.51	8.16
	9	27.28	43.99	12.02	24.05	6.81	14.43	6.42	13.73

UCS: Uniaxial compressive strength, p: Cutting depth, F_c: Mean cutting force, F'_c: Peak cutting force.

3.3. Effect of the Rake Angle on the Cutting Force

The effect of the rake angle was also investigated by the analysis of the mean cutting force and peak cutting force.

Figure 11 plots the mean cutting force with respect to the rake angle. When the rake angle increases from 0° to 5°, the cutting force decreases slightly. At a cutting depth of 3 mm, it reduced by 0.15 kN from 2.59 kN to 2.44 kN and by 0.06 kN from 0.94 kN to 0.88 kN the for UCS 50 MPa and decreased UCS 30 MPa rocks, respectively (Figure 11a). Similarly, at a cutting depth of 9 mm, it reduced from 10.18 kN to 9.07 kN and 5.25 kN to 5.11 kN for the UCS 50 MPa and UCS 30 MPa rocks, respectively (Figure 11c).

However, when the rake angle increased above 5°, the mean cutting force increased. When the rake angle increased from 5° to 15° at a cutting depth of 6 mm, the mean cutting force of the UCS 40 MPa and UCS 20 MPa rocks increased from 3.53 kN to 5.07 kN and 1.42 kN to 2.12 kN, respectively (Figure 11b).

The peak cutting force exhibits similar trends (Figure 12). At a cutting depth of 6 mm, the cutting force of the UCS 50 MPa rock decreases from 11.55 kN to 9.38 kN as the rake angle increases from 0° to 5°. In addition, when the rake angle increases from 5° to 15°, the peak cutting force increases to 12.85 kN (Figure 12b).

This phenomenon also appears to be caused by friction between the cutting tool and rock. Figure 13 shows the friction surface of the cutting tool after cutting, which increases slightly with the rake angle. The details of the mean and peak cutting forces according to the rake angle are listed in Table 4.

In summary, the cutting force decreased with increasing clearance angles. In particular, when the angle increased from 0° to 5°, the cutting force decreased significantly. Furthermore, when it exceeded 10°, the cutting force converged to a constant value. However, the cutting force increased with the rake angle. A slight decrease occurred when increased from 0° to 5°, but an increase was observed after that. However, the effect of the rake angle was significantly lower than that of the clearance angle.

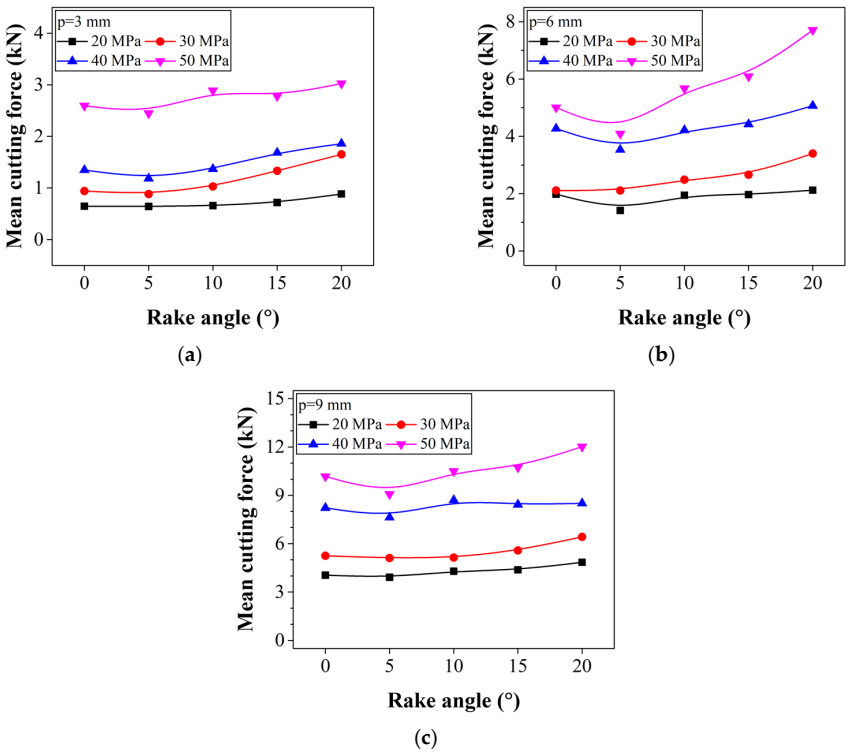

Figure 11. Relationship between the mean cutting force and rake angle at cutting depths (*p*) of: (**a**) 3 mm, (**b**) 6 mm, and (**c**) 9 mm.

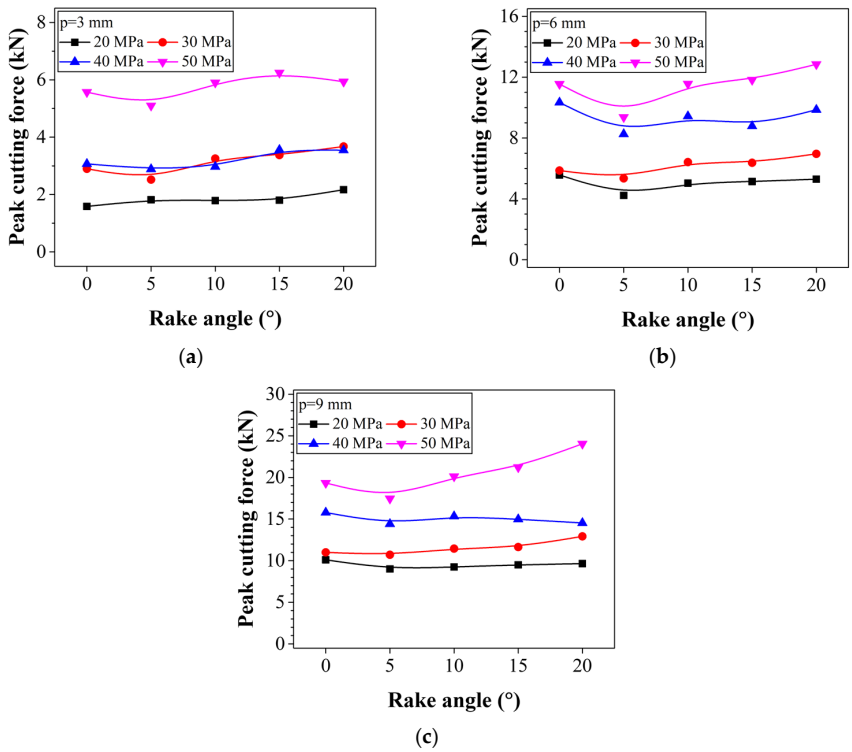

Figure 12. Relationship between the peak cutting force and rake angle for depths (*p*) of: (**a**) 3 mm, (**b**) 6 mm, and (**c**) 9 mm.

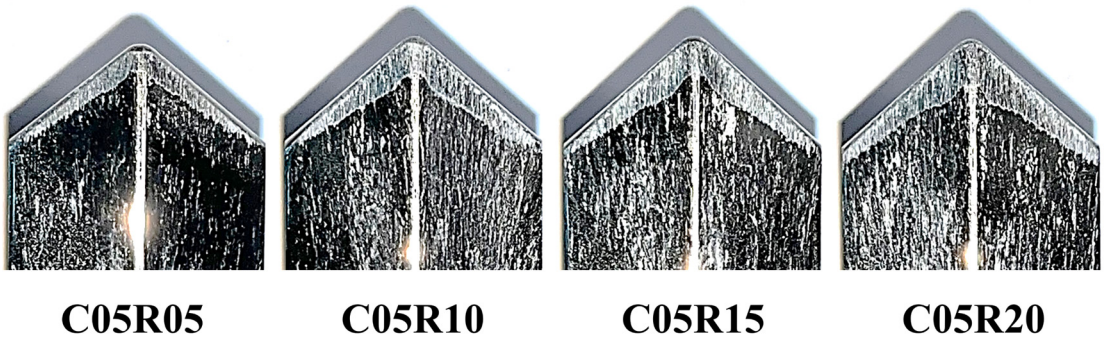

Figure 13. Friction surface of the cutting tool after the cutting test.

Table 4. Mean and peak cutting forces for various rake angles.

UCS (MPa)	p (mm)	Rake Angle (Deg.)									
		0		5		10		15		20	
		F_c (kN)	F'_c (kN)	F_c (kN)	F'_c (kN)	F_c (kN)	F'_c (kN)	F_c (kN)	F'_c (kN)	F_c (kN)	F'_c (kN)
20	3	0.65	1.59	0.64	1.82	0.66	1.79	0.72	1.80	0.88	2.17
	6	1.98	5.57	1.42	4.23	1.95	5.03	1.97	5.14	2.12	5.30
	9	4.04	10.11	3.91	9.01	4.29	9.24	4.38	9.50	4.84	9.65
30	3	0.94	2.90	0.88	2.52	1.03	3.25	1.33	3.38	1.65	3.68
	6	2.11	5.86	2.11	5.35	2.49	6.42	2.66	6.37	3.40	6.96
	9	5.25	11.00	5.11	10.71	5.14	11.45	5.58	11.64	6.42	12.92
40	3	1.35	3.07	1.18	2.89	1.37	2.97	1.69	3.56	1.86	3.55
	6	4.27	10.34	3.53	8.26	4.22	9.43	4.43	8.78	5.07	9.86
	9	8.22	15.79	7.62	14.41	8.71	15.34	8.43	14.98	8.50	14.54
50	3	2.59	5.57	2.45	5.10	2.89	5.90	2.78	6.25	3.02	5.94
	6	5.01	11.55	4.09	9.38	5.67	11.57	6.09	11.83	7.71	12.85
	9	10.18	19.33	9.07	17.46	10.50	20.12	10.73	21.22	12.02	24.05

UCS: Uniaxial compressive strength, p: Cutting depth, F_c: Mean cutting force, F'_c: Peak cutting force.

3.4. Effect of the Cutting Volume

The fragment recovery method [22] and sand-filling method [23] were used to measure the cutting volume in the linear cutting test. The first method measures the weight of rock fragments while the second measures the cutting surface by filling it with sand. In addition, photogrammetry was used to measure the cutting volume [15,23].

In this study, a Calibry mini (a 3D scanner from Thor3d) was used to obtain the cutting volume. This scanner has an accuracy of up to 0.07 mm and can acquire 1,000,000 data points per second. After the cutting was completed, the surface of the deformed rock was scanned to obtain a mesh of the same shape, and the cutting volume was measured using the 3D modeling software Rhino (Figure 14).

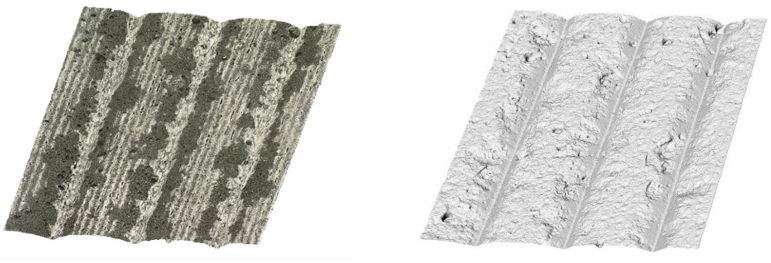

(**a**) (**b**)

Figure 14. 3D scanning with Calibry mini: (**a**) surface of the rock after cutting and (**b**) mesh obtained via 3D scanning.

Figure 15 and Table 5 show the cutting volume according to the clearance angle. The cutting volume decreases as the angle increases, regardless of the cutting depth. At a cutting depth of 3 mm, the cutting volume of the UCS 50 MPa rock sample decreased the most from 4840 mm^3 to 2779 mm^3 as the clearance angle increased from 0° to 15°, and on average, it decreased by 39% (Figure 15a). At cutting depths of 6 mm and 9 mm, the volume decreased by 37% and 24%, respectively, on average (Figure 15b,c, respectively). Thus, it can be concluded that the effect of the cutting volume owing to the clearance angle decreases as the cutting depth increases.

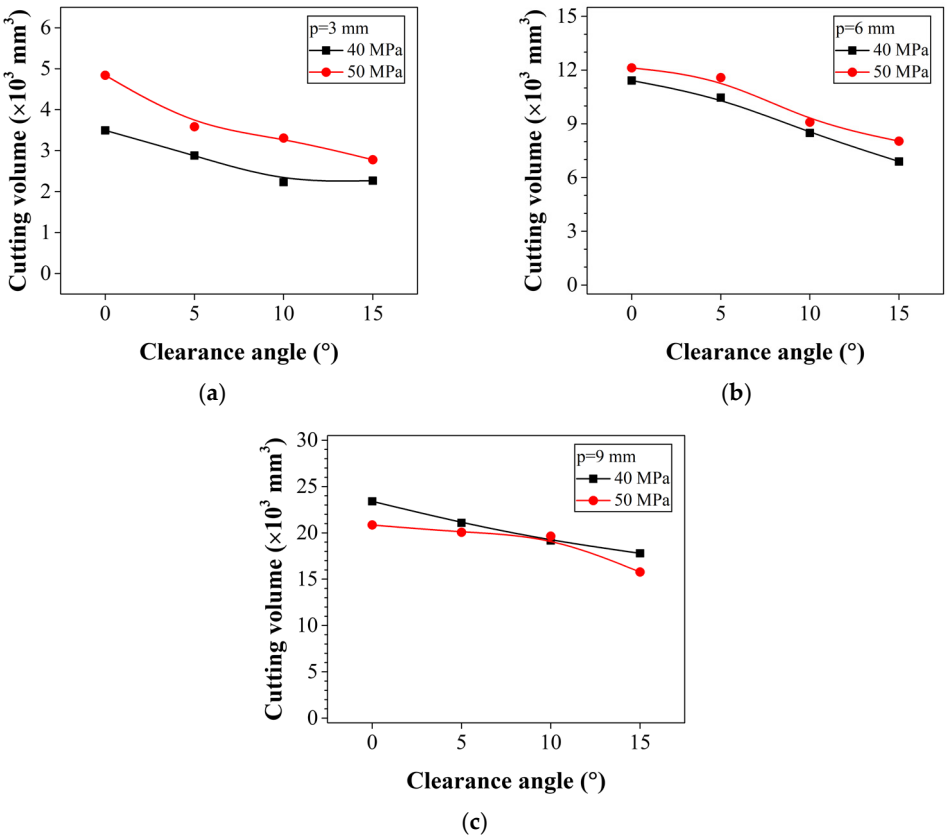

Figure 15. Relationship between the cutting volume and clearance angle for depths (*p*) of: (**a**) 3 mm, (**b**) 6 mm, and (**c**) 9 mm.

Table 5. Cutting volume and specific energy for various clearance angles.

UCS (MPa)	*p* (mm)	Clearance Angle (Deg.)							
		0		5		10		15	
		V_c (mm^3)	SE (MJ/m^3)	V_c (mm^3)	SE (MJ/m^3)	V_c (mm^3)	SE (MJ/m^3)	V_c (mm^3)	SE (MJ/m^3)
40	3	3495	411.0	2880	116.2	2229	122.0	2267	97.9
	6	11,416	194.4	10,463	87.2	8489	78.6	6892	88.1
	9	23,400	208.3	21,082	72.6	19,180	55.5	17,788	47.1
50	3	4840	322.2	3585	151.8	3306	107.2	2779	93.6
	6	12,124	201.8	11,580	119.8	9087	80.2	8030	78.7
	9	20,855	235.4	20,065	107.9	19,638	62.4	15,772	73.3

UCS: Uniaxial compressive strength, *p*: Cutting depth, V_c: Cutting volume, SE: Specific energy.

The variation in the cutting volume according to the rake angle is shown in Figure 16 and listed in Table 6. In all cases, the cutting volume decreases as the rake angle increases from 0° to 5°. When the cutting depth is 3 mm, the cutting volume for UCS 40 MPa

decreases by 23% from 2726 mm^3 to 2102 mm^3. In the case of the 50 MPa UCS, the volume decrease was 12%, from 2574 mm^3 to 2254 mm^3 (Figure 16a). When the cutting depth increases to 9 mm, the reduction rate of the cutting volume decreases to an average of 2% (Figure 16c). Subsequently, as the rake angle increased, the cutting volume also increased, although the amount of change was less than that of the clearance angle.

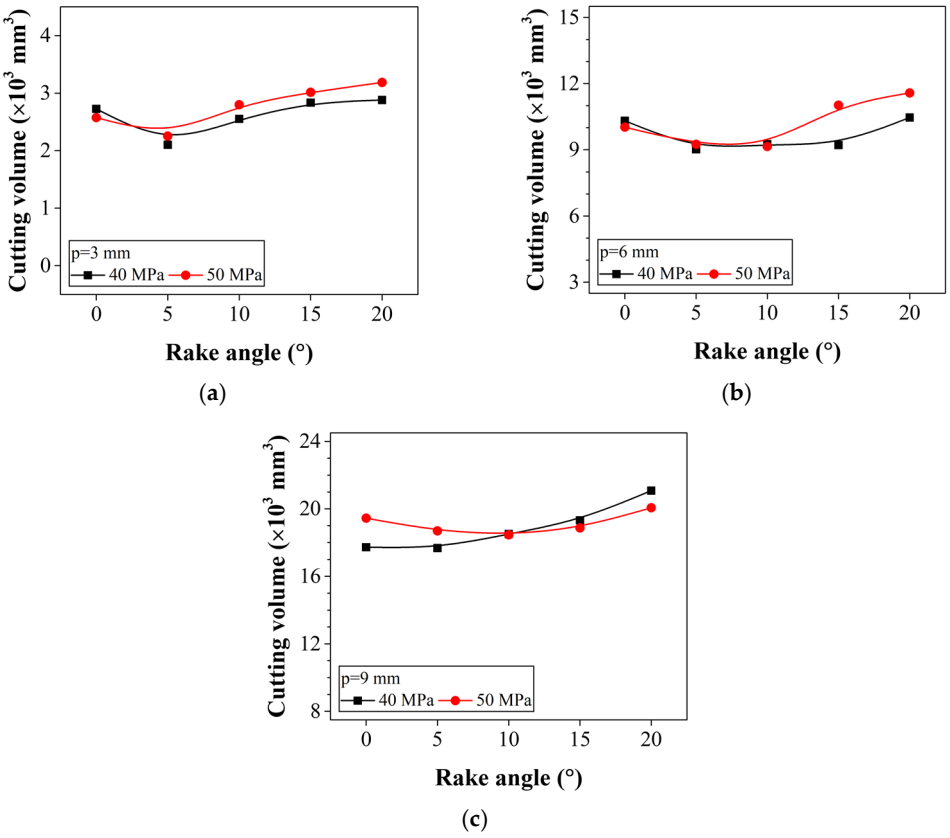

Figure 16. Relationship between the cutting volume and rake angle for depths (*p*) of: (**a**) 3 mm, (**b**) 6 mm, and (**c**) 9 mm.

Table 6. Cutting volume and specific energy for different values of the rake angle.

UCS (MPa)	*p* (mm)	Rake Angle (Deg.)									
		0		5		10		15		20	
		V_c (mm^3)	SE (MJ/m^3)	V_c (mm^3)	SE (MJ/m^3)	V_c (mm^3)	SE (MJ/m^3)	V_c (mm^3)	SE (MJ/m^3)	V_c (mm^3)	SE (MJ/m^3)
40	3	2726	89.0	2102	101.3	2551	96.6	2835	107.0	2880	116.2
	6	10,317	74.5	9026	70.5	9258	82.0	9217	86.4	10,463	87.2
	9	20,744	83.5	17,675	77.6	18,504	84.7	19,323	78.5	21,082	72.6
50	3	2574	181.4	2254	195.4	2799	185.8	3014	166.0	3185	170.9
	6	10,027	89.9	9252	79.6	9150	111.6	11,025	99.5	11,580	119.8
	9	19,448	94.2	18,693	87.3	18,457	102.4	18,866	102.4	20,065	107.9

UCS: Uniaxial compressive strength, *p*: Cutting depth, V_c: Cutting volume, SE: Specific energy.

To summarize the effect on the cutting volume according to the shape of cutting tool, the cutting volume decreased with increasing clearance angle, the rake angle caused a slight decrease when increasing from 0° to 5°, and subsequent increases in angle increased the volume. This phenomenon is similar to that of the cutting force, and the cutting force and cutting volume are observed to be proportional.

Figure 17 shows the relationship between the cutting force and cutting volume obtained from the cutting experiments on the UCS 40 MPa and 50 MPa rocks. Except for the case that the clearance angle is 0°, the cutting force and the cutting volume appear to have a linear relationship. In Figure 17, the point at the right end of each cutting depth indicates a case that the clearance angle is 0°. It is located far to the right from the trend line due to excessive cutting force caused by friction between the cutting tool and rock. Furthermore, as the strength of the rock increases, the cutting force generated when cutting the same volume increases, so the slope of the trend line decreases.

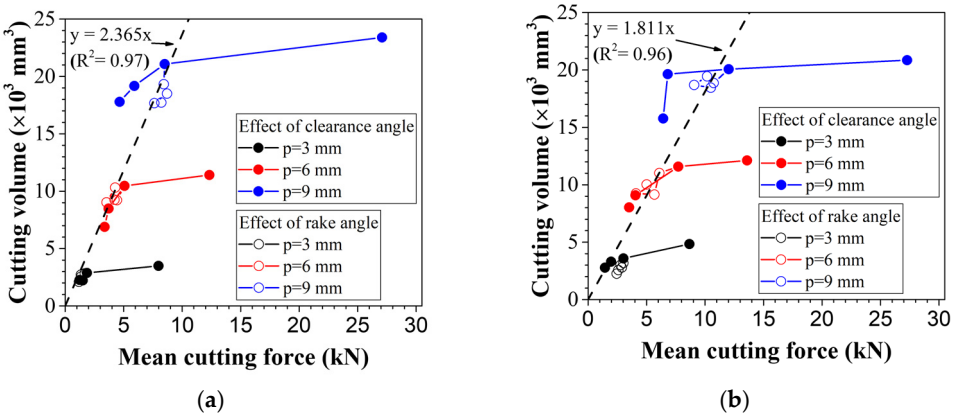

Figure 17. Relationship between the cutting volume and cutting force: (**a**) UCS 40 MPa rock; and (**b**) UCS 50 MPa rock.

3.5. Effect on the Specific Energy

The specific energy is the energy consumed in cutting a unit of volume, and a higher specific energy indicates that more energy is consumed to cut the same volume. Figures 18 and 19 and Tables 5 and 6 show the specific energies according to the clearance and rake angles.

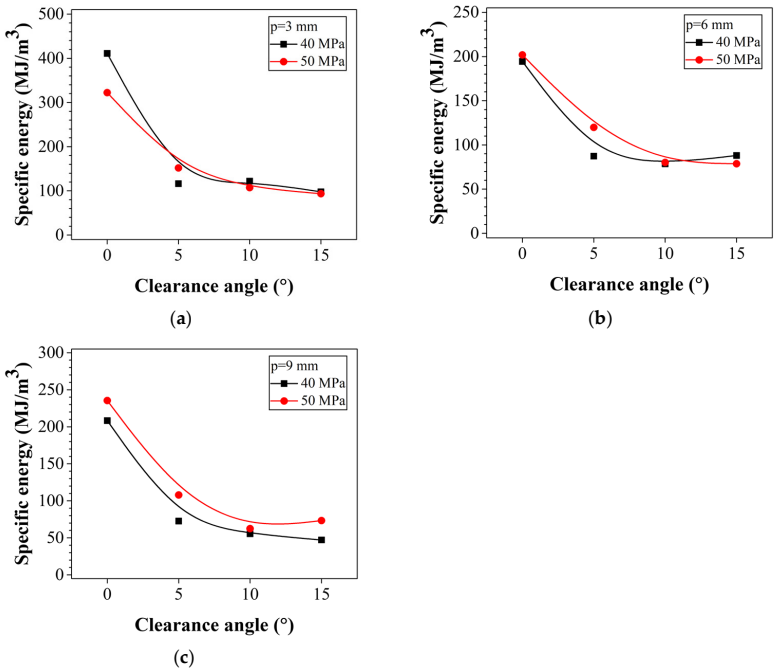

Figure 18. Relationship between the specific energy and clearance angle at depths (*p*) of: (**a**) 3 mm, (**b**) 6 mm, and (**c**) 9 mm.

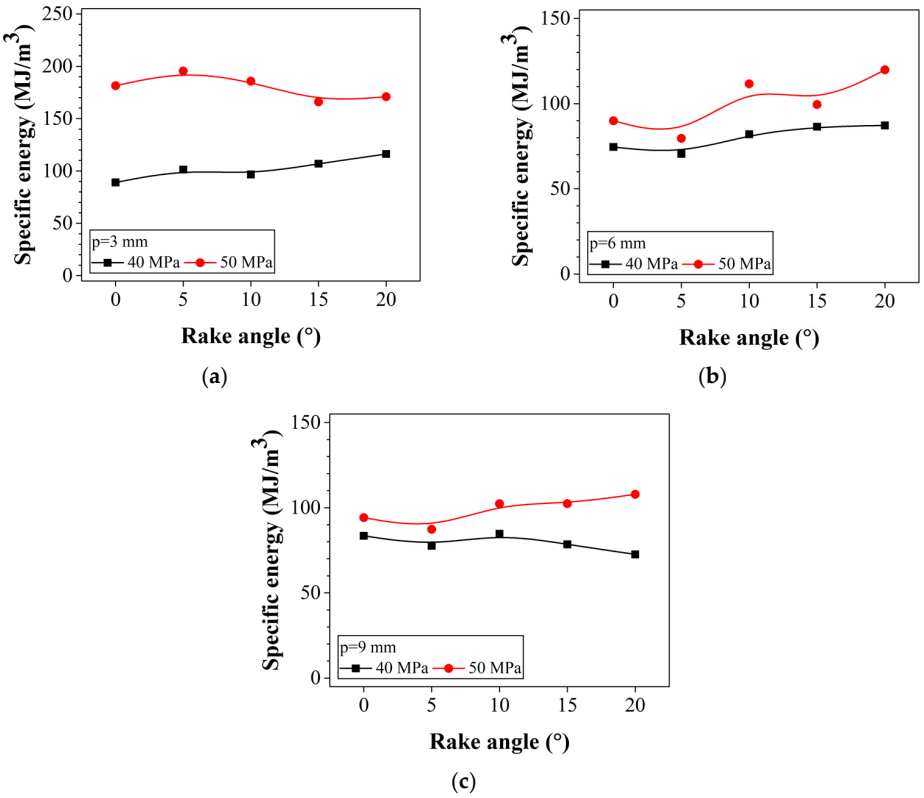

Figure 19. Relationship between the specific energy and rake angle at depths (*p*) of: (**a**) 3 mm, (**b**) 6 mm, and (**c**) 9 mm.

For the clearance angle, the specific energy decreased as the angle increased, and a sharp decrease occurred when it increased from 0° to 5° (Figure 18). When cutting was performed at a depth of 3 mm, the specific energy decreased by 72% and 53% in the rocks with strengths of 40 MPa and 50 MPa, respectively (Figure 18a). When the angle increases from 10°, the specific energy appears to converge to a constant value. When cutting was performed to a depth of 6 mm, the specific energies of both the UCS 40 MPa and 50 MPa rocks converged to approximately 80 MJ/m^3 (Figure 18b).

For the rake angle, no remarkable characteristic was found compared to the effect of the clearance angle; however, the specific energy tended to increase with the angle (Figure 19).

4. Conclusions

In this study, a linear cutting test was performed using the clearance and rake angles as the main variables to analyze the effect of the shape of the cutting tool of the pre-cutting machine. This study can be used as a reference to determine the cutting tool of the pre-cutting machine. The conclusions are as follows:

1. The cutting force and clearance angle have an inverse relationship, and this relation is sharp as the angle increases from 0° to 5°. This sharp reduction occurs because of a dramatic decrease in the friction surface between the cutting tool and rock. Furthermore, when the angle exceeded 10°, it appeared to converge to a certain value.
2. Similar to the cutting force, the clearance angle and cutting volume are inversely related; however, unlike the cutting force, the cutting volume decreases linearly as the angle increases. The specific energy decreased significantly from 0° to 5° and seemed to converge to a constant value after 10°, similar to the cutting force.
3. The relationship between the rake angle and cutting force was direct and indirect before and after 5°, respectively. When the rake angle was increased from 0° to 5°, the cutting force decreased slightly. However, it increased subsequently owing to the increase in the friction surface of the cutting tool.

4. As the rake angle increases, the cutting volume also increases, similar to the cutting force. Even when the rake angle increased from 0° to 5°, the cutting volume decreased slightly, similar to the cutting force. Subsequently, the volume increased with the angle. The specific energy also showed an increasing trend with increasing angles.
5. Finally, the effect of the shape of the cutting tool appears to be mainly due to the friction between the cutting tool and rock. Among the shape variables of the cutting tool, the clearance angle has a greater effect on the cutting force, cutting volume, and specific energy. In addition, the linear relationship between the cutting force and cutting volume was confirmed.

Author Contributions: H.-e.K. proposed the concept of the research and developed the study. K.-m.N. and H.R. contributed to the review of the final manuscript and made recommendations for paper revision. T.K. conducted the experiments and provided suggestions for the experiment. H.-k.Y. supervised the study and provided important suggestions. All authors have read and agreed to the published version of the manuscript.

Funding: This work was supported by a National Research Foundation of Korea grant funded by the Korean Government (NRF-2019R1A2C2003636).

Institutional Review Board Statement: Not applicable.

Informed Consent Statement: Not applicable.

Data Availability Statement: Not applicable.

Conflicts of Interest: The authors declare no conflict of interest.

References

1. van Walsum, E. Mechanical Pre-cutting, A Rediscovered Tunneling Technique. *Rock Mech. Rock Eng.* **1991**, *24*, 65–79. [CrossRef]
2. Wang, T.; Wang, X.; Tan, Z.; Li, K.; He, M. Studies on ground settlement and pre-arching stress of pre-cutting tunnelling method. *Tunn. Undergr. Space Technol.* **2018**, *82*, 199–210. [CrossRef]
3. Bougard, J.F. The mechanical pre-cutting method. *Tunn. Undergr. Space Technol.* **1988**, *3*, 163–167. [CrossRef]
4. Lunardi, G.; Belfiore, A.; Selleri, A.; Trapasso, R. Widening the "Montedomini" tunnel in the presence of traffic: The evolution of the "Nazzano" method. In Proceedings of the ITA-AITES World Tunnel Congress 2014 (WTC 2014), Foz do Iguaçu, Brazil, 9–14 May 2014; pp. 1–10.
5. Lunardi, G.; Agresti, S.; Basta, D. The widening of the "Montedomini" A14 Motorway Tunnel in the presence of traffic. In Proceedings of the ITA-AITES World Tunnel Congress 2016 (WTC 2016), San Francisco, CA, USA, 22–28 April 2016; pp. 1–10.
6. Yasar, S.; Yilmaz, A.O. Drag Pick Cutting Tests: A comparison between experimental and theoretical results. *J. Rock Mech. Geomech. Eng.* **2018**, *10*, 893–906. [CrossRef]
7. Rostami, J.; Ozdemir, L.; Nilson, B. Comparison between CMS and NTH hard rock TBM performance prediction models. In Proceedings of the Annual Technical Meeting of the Institute of Shaft Drilling and Technology (ISDT), Las Vegas, NV, USA, 1–3 May 1996; pp. 1–11.
8. Roxborough, F.F.; Phillips, H.R. Rock excavation by disc cutter. *Int. J. Rock Mech. Min. Sci. Geomech. Abstr.* **1975**, *12*, 361–366. [CrossRef]
9. Rostami, J.; Ozdemir, L. A New Model for Performance Prediction of Hard Rock TBMs. In Proceedings of the Rapid Excavation and Tunneling Conference, Boston, MA, USA, 13–17 June 1993; pp. 793–809.
10. Balci, C.; Tumac, D. Investigation into the effects of different rocks on rock cuttability by a V-type disc cutter. *Tunn. Undergr. Space Technol.* **2012**, *30*, 183–193. [CrossRef]
11. Tumac, D.; Balci, C. Investigations into the cutting characteristics of CCS type disc cutters and the comparison between experimental, theoretical and empirical force estimations. *Tunn. Undergr. Space Technol.* **2015**, *45*, 84–98. [CrossRef]
12. Nishimatsu, Y. The mechanics of rock cutting. *Int. J. Rock Mech. Min. Sci.* **1972**, *9*, 261–270. [CrossRef]
13. Wang, X.; Wang, Q.F.; Liang, Y.P.; Su, O.; Yang, L. Dominant cutting parameters affecting the specific energy of selected sandstones when using conical picks and the development of empirical prediction models. *Rock Mech. Rock Eng.* **2018**, *51*, 3111–3128. [CrossRef]
14. Aresh, B.; Khan, F.N.; Haider, J. Experimental investigation and numerical simulation of chip formation mechanisms in cutting rock-like materials. *J. Petrol. Sci. Eng.* **2022**, *209*, 109869. [CrossRef]
15. Cho, J.W.; Jeon, S.; Jeong, H.-k.Y.; Chang, S.H. Evaluation of Cutting Efficiency during TBM disc cutter excavation within a Korean granitic rock using linear-cutting-machine testing and photogrammetric measurement. *Tunn. Undergr. Space Technol.* **2013**, *35*, 37–54. [CrossRef]

16. Zhang, X.; Xia, Y.; Tan, Q.; Wu, D. Comparison study on the rock cutting characteristics of disc cutter under free-face-assisted and conventional cutting methods. *KSCE J. Civil Eng.* **2018**, *22*, 4155–4162. [CrossRef]
17. Copur, H.; Bilgin, N.; Balci, C.; Tumac, D.; Avunduk, E. Effects of different cutting patterns and experimental conditions on the performance of a conical drag tool. *Rock Mech. Rock Eng.* **2017**, *50*, 1585–1609. [CrossRef]
18. Wang, S.; Li, X.; Du, K.; Wang, S. Experimental investigation of hard rock fragmentation using a conical pick on true triaxial test apparatus. *Tunn. Undergr. Space Technol.* **2018**, *79*, 210–223. [CrossRef]
19. Li, B.; Zhang, B.; Hu, M.; Liu, B.; Cao, W.; Xu, B. Full-scale linear cutting tests to study the influence of pre-groove depth on rock-cutting performance by TBM disc cutter. *Tunn. Undergr. Space Technol.* **2022**, *122*, 104366. [CrossRef]
20. Wang, S.; Sun, L.; Li, X.; Zhou, J.; Du, K.; Wang, S.; Khandelwal, M. Experimental investigation and theoretical analysis of indentations on cuboid hard rock using a conical pick under uniaxial lateral stress. *Geomech. Geophys. Geo-Energy Geo-Resour.* **2022**, *8*, 1–23. [CrossRef]
21. Li, H.S.; Liu, S.Y.; Xu, P.P. Numerical simulation on interaction stress analysis of rock with conical picks. *Tunn. Undergr. Space Technol.* **2019**, *85*, 231–242. [CrossRef]
22. Snowdon, R.A.; Ryley, M.D.; Temporal, J. A study of disc cutting in selected British rocks. *Int. J. Rock Mech. Min. Sci. Geomech. Abstr.* **1982**, *19*, 107–121. [CrossRef]
23. Cho, J.W. Linear Cutting Test and Numerical Study on the Assessment of Rock Cuttability of a TBM Disc Cutter. Ph.D. Thesis, Seoul National University, Seoul, Korea, 2010.